



Salinization in a stratified aquifer induced by heat transfer from well casings



Jan H. van Lopik^{a,b,*}, Niels Hartog^{a,b}, Willem Jan Zaadnoordijk^{b,c}, D. Gijsbert Cirkel^b, Amir Raoof^a

^a Utrecht University, Department of Earth Sciences, Budapestlaan 4, 3584 CD Utrecht, The Netherlands

^b KWR Watercycle Research Institute, Groningenhaven 7, 3433 PE Nieuwegein, The Netherlands

^c Delft University of Technology, Water Resources Section, Faculty of Civil Engineering and Geosciences, Stevinweg 1, 2628 CN Delft, The Netherlands

ARTICLE INFO

Article history:

Received 21 January 2015

Revised 24 September 2015

Accepted 25 September 2015

Available online 9 October 2015

Keywords:

Thermo-haline convection

Wellbore heat transmission

Salinization

Non-linear density equation

SEAWAT

ABSTRACT

The temperature inside wells used for gas, oil and geothermal energy production, as well as steam injection, is in general significantly higher than the groundwater temperature at shallower depths. While heat loss from these hot wells is known to occur, the extent to which this heat loss may result in density-driven flow and in mixing of surrounding groundwater has not been assessed so far. However, based on the heat and solute effects on density of this arrangement, the induced temperature contrasts in the aquifer due to heat transfer are expected to destabilize the system and result in convection, while existing salt concentration contrasts in an aquifer would act to stabilize the system. To evaluate the degree of impact that may occur under field conditions, free convection in a 50-m-thick aquifer driven by the heat loss from penetrating hot wells was simulated using a 2D axisymmetric SEAWAT model. In particular, the salinization potential of fresh groundwater due to the upward movement of brackish or saline water in a stratified aquifer is studied. To account for a large variety of well applications and configurations, as well as different penetrated aquifer systems, a wide range of well temperatures, from 40 to 100 °C, together with a range of salt concentration (1–35 kg/m³) contrasts were considered. This large temperature difference with the native groundwater (15 °C) required implementation of a non-linear density equation of state in SEAWAT. We show that density-driven groundwater flow results in a considerable salt mass transport (up to 166,000 kg) to the top of the aquifer in the vicinity of the well (radial distance up to 91 m) over a period of 30 years. Sensitivity analysis showed that density-driven groundwater flow and the upward salt transport was particularly enhanced by the increased heat transport from the well into the aquifer by thermal conduction due to increased well casing temperature, thermal conductivity of the soil, as well as decreased porosity values. Enhanced groundwater flow and salt transport was also observed for increased hydraulic conductivity of the aquifer. While advective salt transport was dominant for lower salt concentration contrasts, under higher salt concentration contrasts transport was controlled by dispersive mixing at the fresh-salt water interface between the two separate convection cells in the fresh and salt water layers. The results of this study indicate heat loss from hot well casings can induce density-driven transport and mixing processes in surrounding groundwater. This process should therefore be considered when monitoring for long-term groundwater quality changes near wells through which hot fluids or gases are transported.

© 2015 Elsevier Ltd. All rights reserved.

1. Introduction

Oil and gas deposits, as well as exploitable geothermal energy, are typically found in reservoirs well below the depths of exploitable fresh groundwater supplies. Therefore, wells for conventional oil

and gas, shale gas and geothermal energy production fully penetrate shallow fresh water aquifers. The temperatures of wellbores during oil production [6], gas production [11], geothermal energy production [13] and hot water or steam injection [50], can be significantly higher (e.g., $T > 40$ °C) than the typical temperatures of the shallow aquifers in moderate climates (10–20 °C). The temperature difference causes heat transfer to the surrounding formations and cooling of the fluid or gas that is flowing inside the well [35]. The resulting temperature at the wellhead is important for operational drilling and injection/production aspects, such as determining viscosity and

* Corresponding author at: Utrecht University, Department of Earth Sciences, Environmental Hydrogeology Group, Budapestlaan 4, 3584 CD Utrecht, The Netherlands. Tel: +31 631697963.

E-mail address: j.h.vanlopik@gmail.com, j.h.vanlopik@uu.nl (J.H. van Lopik).

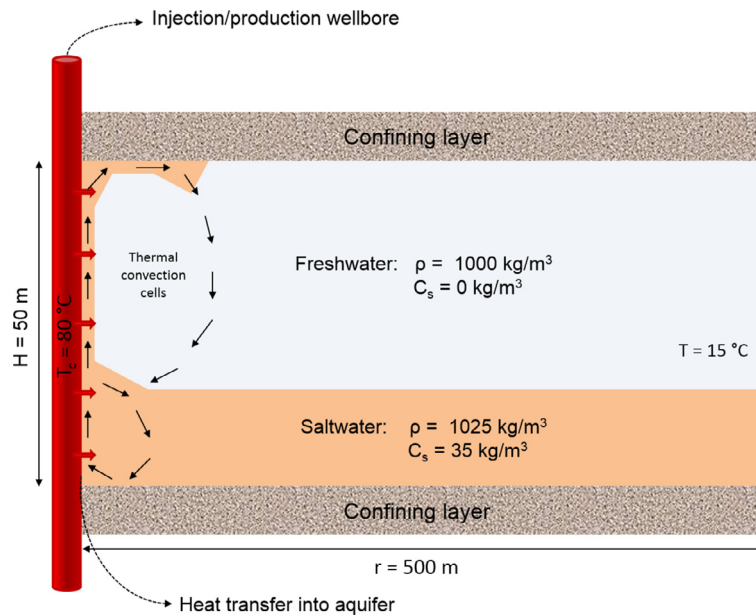


Fig. 1. Thermally induced density-driven flow due to heat transfer from a well to the aquifer and its effect on fresh-salt stratified groundwater (parameter values belong to the reference scenario used in this study).

thereby flowing pressure changes in a heavy-oil well, or estimating steam quality during steam injection. However, to our knowledge, the thermal effects of wellbore heat losses for the aquifers that receive the heat have not been addressed.

Many studies have investigated density-driven flow in porous media under the influence of temperature contrasts in groundwater systems (e.g. [4,15]). This can occur both at large scale, like geothermal convection in geological basins [4], or at small scale such as the upward density-driven flow of injected hot water during high temperature aquifer thermal energy storage (e.g. [2,27,42,44]). In addition to temperature, density-driven groundwater flow is affected by salt concentration contrasts. The effect of salt concentration and temperature gradients on convective flow patterns in thermo-haline systems were studied by [4,17,29,36,39]. A few studies have focused on thermo-haline convection on field scale; e.g. the effect of hypersaline cooling canals on aquifer salinization [16] and the transport of hot, brine water plumes [30].

Thermal convection under the influence of a vertical heat source like a vertical flat plate [3] or long vertical thin blades [32] in a porous medium has been investigated numerically. These geophysical examples suggest that hot wellbores penetrating cooler aquifers could thermally induce density-driven groundwater flow.

In many aquifers, fresh groundwater overlies denser, saline water and salinization by mobilization of the underlying saline water is considered a major threat to fresh groundwater resources and drinking water production [5,34,48]. Local thermally induced density-driven flow in the vicinity of hot well casings could therefore result in mixing and deterioration of the groundwater quality (see Fig. 1). To explore this possibility, we simulated transient temperature and salinity dependent density-driven groundwater flow along a hot wellbore. We used SEAWATv4, and further include a non-linear density equation of state, to apply to various thermal conditions, salt concentration contrasts and aquifer properties.

2. Theory and methodology

2.1. Wellbore heat transmission

Fluid or gas flowing in the wellbore loses heat to its surroundings by thermal conduction due to the difference between wellbore fluid

and surrounding aquifer temperature during injection or production operations. The heat transfer from the wellbore is proportional to the thermal resistance of the well system, including the tubing wall, annulus, casing wall and cement sheets. Ramey [35] introduced an approximate, analytical solution for wellbore heat transmission to estimate wellhead temperature as a function of wellbore depth and the operational time. He has developed solutions for fluids and perfect gasses, assuming steady-state fluid flow in the wellbore and transient heat conduction into the formation. An overall heat transfer coefficient was introduced to account for the total thermal resistance of the well system. Other studies introduced methods to account for multiple formation layers with different physical properties [50], for real gas production [11], or for two-phase flow in the wellbore [13]. Wellhead temperature distributions during oil, gas and geothermal energy production, as well as temperature distributions of steam and hot water injection applications, show that the difference between wellbore fluid temperature and surrounding formation at shallow depths can be significant with temperature differences larger than 30°C [6,11,13,35,50]. However, the effective temperature of the outer well casing may differ from the wellbore fluid temperature, depending on the total thermal resistance of the well system. In general, thermal resistance of steel casings and tubings can be neglected, while insulating materials like cement sheets and annuli filled with liquid or gas have a high thermal resistance. According to Ramey [35], heat transfer through the different thermal resistance elements of the wellbore is considerably faster than heat transfer in the surrounding formation and, therefore, may be assumed as a steady-state solution.

2.2. SEAWAT

We have used SEAWATv4 [10,24] to model density-driven groundwater flow induced by heat transfer from a hot well casing. SEAWATv4 is a coupled version of the simulation programs for groundwater flow, MODFLOW2000 [12] and for multi-species mass transport, MT3DMS [51], together with a variable density and viscosity package. This enables the simulation of variable-density groundwater flow combined with heat and multi-species solute transport. The differential equation for solute transport takes into

account advection, dispersion and molecular diffusion:

$$\left(1 + \frac{\rho_b K_d}{\theta}\right) \frac{\delta(\theta C)}{\delta t} = \nabla \left[\left(D_m + \alpha \frac{q}{\theta} \right) (\nabla C) \right] - \nabla(qC) - q'_s C_s \quad (1)$$

where C is the concentration of the solute (kg/m^3), t is the time (d), q is the specific discharge, ρ_b is the bulk density (kg/m^3), K_d is the distribution coefficient (m^3/kg), D_m is the molecular diffusion coefficient (m^2/d), θ is the porosity, α (m) is the dispersivity coefficient, q_s is the source or sink (m/d) and C_s is the source or sink concentration (kg/m^3). We have followed Langevin [24] and employed solute transport equations to simulate heat transport in the aquifer:

$$\begin{aligned} & \left(1 + \frac{1-\theta}{\theta} \frac{\rho_s c_{ps}}{\rho c_{pf}}\right) \frac{\delta(\theta T)}{\delta t} \\ &= \nabla \left[\left(\frac{\lambda_f \theta + (1-\theta)\lambda_s}{\theta \rho c_{pf}} + \alpha \frac{q}{\theta} \right) (\nabla T) \right] - \nabla(qT) - q'_s T_s \end{aligned} \quad (2)$$

The molecular diffusion coefficient, as input parameter, can be used to describe conductive heat transport by defining a bulk thermal diffusivity, D_T (m^2/d), as:

$$D_T = \frac{\lambda_f \theta + (1-\theta)\lambda_s}{\theta \rho c_{pf}} \quad (3)$$

where λ_f and λ_s ($\text{W/m}^\circ\text{C}$) are the thermal conductivity of water and solid phase, respectively, c_{pf} is the heat capacity of water ($\text{J/kg}^\circ\text{C}$) and ρ is the water density (kg/m^3). Moreover, thermal equilibrium between water and the solid phase during heat transport is represented by a thermal distribution factor, K_{dT} (m^3/kg):

$$K_{dT} = \frac{c_{ps}}{\rho c_{pf}} \quad (4)$$

where c_{ps} ($\text{J/kg}^\circ\text{C}$) is the heat capacity of solid phase. Therefore, thermal retardation can be described in a similar manner as solute retardation:

$$R_T = 1 + \frac{\rho_b}{\theta} K_{dT} \quad \text{where } \rho_b = \rho_s(1-\theta) \quad (5)$$

where ρ_s (kg/m^3) is the solid phase density.

SEAWATv4 uses the Oberbeck–Boussinesq approximation (e.g. [4]) to assume a constant fluid density in the heat transport equation, while fluid density is a function of salt concentration and temperature in the buoyancy term [40]. Assuming a constant fluid density (ρ) and the heat capacity of the fluid (c_{pf}) simplifies the heat transport equation (Eq. (2)) and enables the use of a constant bulk thermal diffusivity (D_T) and thermal distribution factor (K_{dT}). We have used a fluid density (ρ) of 1000 kg/m^3 to calculate these parameters. At high temperature and salt concentration contrasts the Oberbeck–Boussinesq approximation becomes insufficient [4,21]. In our simulated scenarios large temperature contrasts between well casing (80°C) and background groundwater temperatures are used, as well as large salt concentration contrasts (0 – 35 kg/m^3). Maximum fluid density is that of seawater ($C_s = 35 \text{ kg/m}^3$) at a temperature of 15°C with a value of 1027 kg/m^3 . Close to the wellbore, the water is heated up to 71.5°C , resulting in a fluid density of 977 kg/m^3 . Considering these densities, the likely change in the bulk thermal diffusivity term (D_T) and the thermal distribution factor (K_{dT}) can be calculated with Eqs. (3) and (4). The relative error for D_T and K_{dT} is $\pm 2.5\%$ while using the fluid density of 1000 kg/m^3 as a reference. This means that the resulting minimum and maximum D_T values are 0.124 and $0.129 \text{ m}^2/\text{d}$, respectively. For K_{dT} , these values are $1.86 \cdot 10^{-4}$ and $1.96 \cdot 10^{-4} \text{ m}^3/\text{kg}$ and the error in heat transport due to the Oberbeck–Boussinesq approximation will be negligible [40].

The Boussinesq approximation in SEAWAT also simplifies the continuity equation such that the volume of water is not influenced by temperature and salinity, but only by head [21]. This means the source terms $\rho b_T \partial T / \partial t$ and $\rho b_C \partial C / \partial t$ are neglected with respect to $\rho S_s \partial h / \partial t$, where b_T and b_C are the thermal and solute coefficient of

water expansivity, respectively. Our study has ranges of temperature from 20 to 60°C , salinity from 0 to 35 kg/m^3 , and head variation of 0.5 m . Using values of $b_T = 4.3 \cdot 10^{-4} ^\circ\text{C}^{-1}$ and $b_C = 7.3 \cdot 10^{-4} \text{ m}^3/\text{kg}$, this means this assumption is not warranted. However, the volume changes do not have a large influence on the flow in our study. The influences on the volume are strongest near the well, uniformly over the thickness of the aquifer. The related pressure changes dissipate laterally so that the upward convection along the well hardly is affected.

2.3. Equation of state

Equations of state describe the temperature and salinity dependence of properties of water, such as density, viscosity, heat capacity, and thermal conductivity. SEAWATv4 allows for equations of state for fluid density and viscosity. The following viscosity equation [46] is used in SEAWAT:

$$\mu(C, T) = 2.394 \cdot 10^{-5} \cdot \left(10^{\frac{248.37}{T+133.15}} \right) + 1.92 \cdot 10^{-6} (C - C_0) \quad (6)$$

where μ is the dynamic viscosity (kg/m s), C is the salt concentration (kg/m^3) and T is the temperature of the fluid.

The current standard SEAWATv4 computer code allows only for a linearized form of the density equation of state:

$$\rho = \rho_f + \frac{d\rho}{dC} (C - C_0) + \frac{d\rho}{dT} (T - T_0) \quad (7)$$

This linear form of the density equation of state is used in many groundwater flow and heat transport codes, like SUTRA [46] and HST3D [20]. However, the density–temperature relationship is indeed non-linear (e.g. [26,37,38,41,49]). It can only be linearized with a $\delta\rho/\delta T$ error of less than 5% for temperature ranges in the order of 2°C for low water temperatures ($\sim 20^\circ\text{C}$) and for temperature ranges in the order of 10°C for higher water temperatures ($\sim 60^\circ\text{C}$) (see Fig. 2). For a wide range of temperature and salinity, Sharqawy et al. [38] derived an empirical non-linear density relationship based on experimentally derived datasets for both salinity and temperature at 1 atm pressure from Isdale and Morris [18] and Millero and Poisson [26]:

$$\begin{aligned} \rho(T, S) = & (999.9 + 2.034 \cdot 10^{-2} T - 6.162 \cdot 10^{-3} T^2 \\ & + 2.261 \cdot 10^{-5} T^3 - 4.657 \cdot 10^{-8} T^4) \\ & + \left(\frac{802.05}{1000} - 2.001 \frac{S}{1000} T + 1.677 \cdot 10^{-2} \frac{S}{1000} T^2 \right. \\ & \left. - 3.060 \cdot 10^{-5} \frac{S}{1000} T^3 - 1.613 \cdot 10^{-5} \left(\frac{S}{1000} \right)^2 T^2 \right) \end{aligned} \quad (8)$$

where S is the salinity (g/kg) and T is the temperature ($^\circ\text{C}$). This density relationship (Fig. 3) is valid for a temperature range of 0 – 180°C and a salinity range of 0 – 160 g/kg with an accuracy of $\pm 0.1\%$.

Previous simulation studies on density-driven groundwater flow have used different density equations of state (Table 1). Thorne et al. [40] and Langevin et al. [25] verified SEAWATv4 by modeling the Henry–Hilleke problem with the temperature and salt concentration ranges shown in Fig. 3. Their linear approximations for the density–temperature relationship are shown in Fig. 2. Holzbecher [15] and Tsang et al. [42] have used a non-linear density–temperature relationship (Table 1) based on empirical relationships derived by Tilton and Taylor [41] and Wooding [49], respectively.

The conditions for density-driven groundwater flow in our study span large temperature contrasts between a well casing (up to 100°C) and background groundwater temperatures of 15°C , as well as large salt concentration contrasts (0 – 35 kg/m^3). First, we have investigated the effect of using a non-linear density equation in the SEAWATv4 code for the reference scenario (Case 1) and compared these results with a scenario run with the conventional SEAWATv4 code using the linear density equation of state (Case 1.1). A linear density–temperature approximation for the conditions considered in this

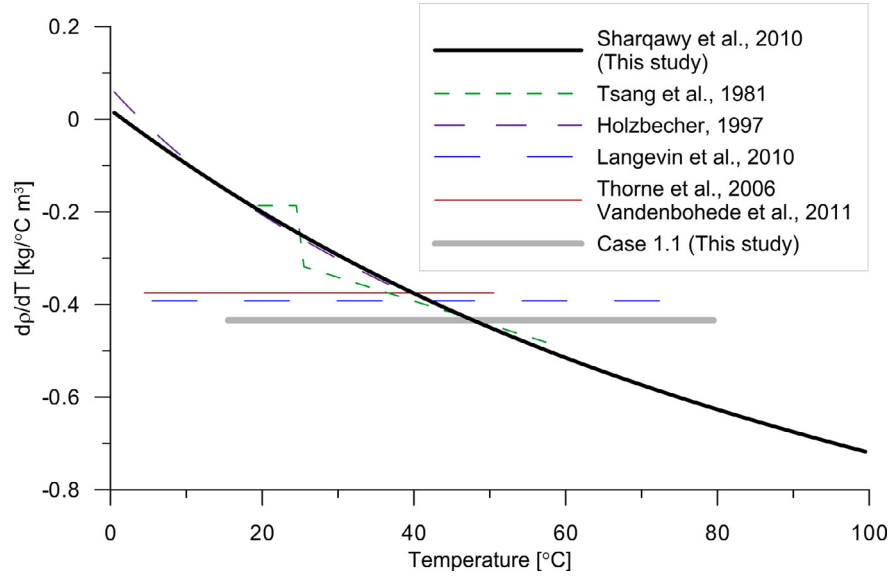


Fig. 2. Dependence of density–temperature gradient on temperature based on the density equation of state as listed for each study in Table 1, while considering fresh water ($S = 0$ g/kg). The gray line shows the linear approximation over the temperature range 15–80 °C at a salinity value of 17.5 g/kg based on Eq. (8) [38]. These $d\rho/dT$ gradient is used for our modeling study (Case 1.1).

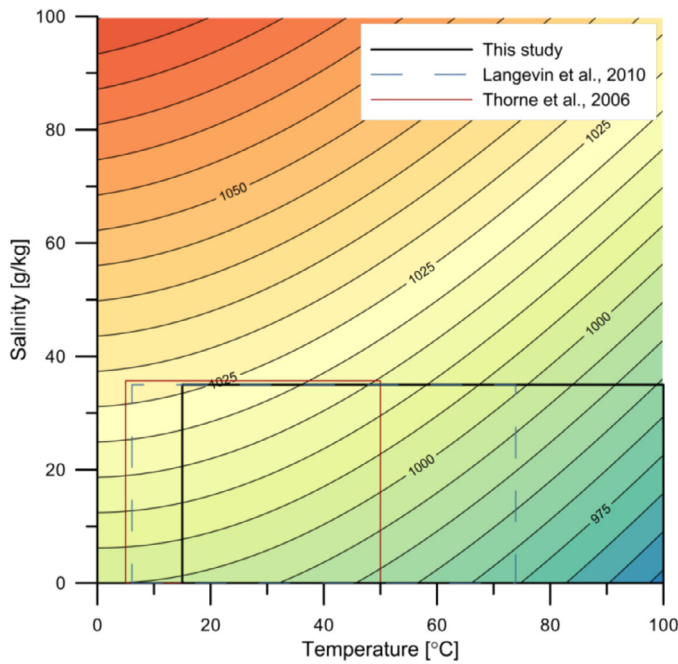


Fig. 3. Water density [kg/m³] at different temperature and salinity values calculated with Eq. (8) [38], where the used salinity and temperature ranges are shown for the studies listed in Table 1 and the present study.

study was derived from Eq. (8) by linear interpolation of the minimum and maximum density values. For the linear approximation of the reference scenario (Case 1.1), the temperature range of 15–80 °C and the average salinity value of the aquifer system (17.5 g/kg) were used. This results in a $d\rho/dT$ gradient of -0.434 (Fig. 2, Case 1.1). The linear density approximation over this temperature range yields a deviation from the non-linear relationship (Eq. (8), with $S = 17.5$ g/kg) at both low and high ends, respectively with an overestimation and underestimation of the density–temperature gradient by approximately a factor 2. To determine the effect of deviations caused by the linearization of the density relationship on modeling density-driven flow, we have also implemented the empirical non-linear equation (Eq. (8)), developed by Sharqawy et al. [38], in the SEAWATv4 code. An iterative algorithm was implemented to calculate the fluid density from the salt concentration (C_s) and temperature (see Fig. 4). Closure of the iterative process was set at a relative density difference of $1 \cdot 10^{-3}$. The source code implementation is given in Appendix A.

2.4. Model setup

We considered a homogeneous confined sandy aquifer with a horizontal interface between fresh and saline groundwater at 40 m depth (10 m above the aquifer bottom). The groundwater flow was simulated axi-symmetrically, following the approach of Langevin [23] which has been validated for transport of solutes [47] and heat [45].

We assumed a constant effective temperature of the outer well casing, to simulate the heat loss from the well. Analytical and field

Table 1
Density equation of state in previous variable-density groundwater modeling studies.

Study	T-range [°C]	C_s -range [kg/m³]	Density equation of state	Code
Langevin et al. [25]	6.1–73.9	0–35	$\rho = 1000 + 0.78C - 0.392(T - 14)$	SEAWAT
Thorne et al. [40]	5–50	0–35.7	$\rho = 1000 + 0.7C - 0.375T$	SEAWAT
Vandenbohede et al. [44]	7.85–48	0	$\rho = 1000 - 0.375(T - 10)$	SEAWAT
Tsang et al. [42]	20–55.4	0	$T > 25$ °C: $\rho = 996.9[1 - 3.17 \cdot 10^{-4}(T - 25) - 2.56 \cdot 10^{-6}(T - 25)^2]$ $T < 25$ °C: $\rho = 996.9[1 - 1.87 \cdot 10^{-4}(T - 25)]$	CCC
Holzbecher [15]	0–40	0	$\rho = (1 - \frac{(T - 3.9863)^2}{508929.2} \cdot \frac{T + 288.9414}{T + 68.12963}) \cdot 1000$	FAST_C(2D)

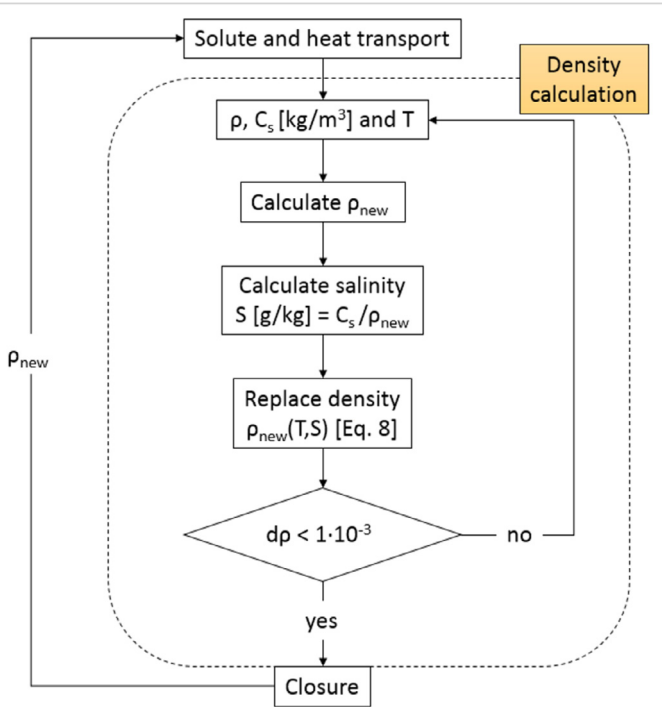


Fig. 4. Flowchart for the non-linear density calculation in the SEAWAT code.

studies have shown that in many cases the bore-face temperature at a given depth can be considered constant [22,35]. The heat transport through the well casing elements can be considered rapid compared to heat transport into the surrounding aquifer and can be considered steady-state [35]. In addition, we assumed that the effective well casing temperature (T_c) is constant over the entire aquifer thickness of only 50 m. Using Ramey's solution [35], this is a reasonable assumption for this limited depth range.

In the axi-symmetric transient model, a radius of 500 m and aquifer thickness of 50 m was used. The grid resolution in the model domain is $\Delta r = 0.25$ m by $\Delta z = 0.5$ m for $[0.5 < r < 23]$, $\Delta r = 0.5$ m by $\Delta z = 0.5$ m for $[23 < r < 180]$ and $\Delta r = 1$ m by $\Delta z = 0.5$ m for

$[180 < r < 500]$. The well system is 0.499 m thick, where the first column, representing the wellbore, is defined as a no-flow boundary. The second column is only 0.001 m thick and represents the outer well casing with a constant effective well casing temperature (T_c). The initial aquifer temperature is 15 °C and the initial salt concentration is 0 kg/m³ for $[0 < z < 40]$ and C_s $[40 < z < 50]$ (see Table 2). The top and bottom are no-flow and no-heat flux boundaries. The outer boundary has a constant temperature, salt concentration and head that equals the initial conditions. The Preconditioned Conjugate Gradient 2 (PCG2) was used to solve for groundwater flow. The method of characteristics (MOC) was applied to solve the advection part of transport, with a Courant number of 0.1. The convergence criterion of relative temperature was set to 10^{-10} °C to simulate heat conduction with a high bulk thermal diffusivity accurately [45].

2.4.1. Model parameters and sensitivity

First, the standard SEAWATv4 with a linear density relation was applied and results for the reference scenario (Table 2) were compared with the results from a simulation with the newly implemented non-linear relation. Subsequently, the non-linear relation was used for the subsequent simulations to investigate the sensitivity of modeling results on the main input variables of well casing temperature (T_c), salt concentration contrasts (C_s), as well as aquifer properties (Table 2). A non-linear density–temperature relation without the density effects of salinity (see Eq. (8), $S = 0$ kg/m³) was used for Case 3.3. The same conditions were assumed as for Case 3.1 with a tracer concentration (C_{tr}) of 1.0 kg/m³ to investigate the effect of small salt concentration gradients on density-driven flow and salt mass transport. The values for aquifer properties were varied within the range expected for sandy aquifers, using Bear [1] and Fitts [8] for hydraulic conductivity and porosity, as well as Molz et al. [27] and the Engineering Toolbox [7] for thermal conductivity and heat capacity. Heterogeneous sandy aquifers with small clay layers could have elevated heat capacities, since average clay heat capacity is 920 J/kg°C [7], which is higher than the value of 800 J/kg°C used for sand. Therefore, a scenario with a higher heat capacity of the aquifer than used for the reference scenario was also considered (Case 6.2). For all scenarios, the viscosity dependence on temperature is taken in account using Eq. (6) in SEAWATv4.

Other hydraulic properties and thermal properties (Table 3) were kept constant between the various simulations. A longitudinal dis-

Table 2

Summary of the input parameters analyzed in the sensitivity analysis. Underlined values indicate a variation on the reference scenario (Case 1).

Case	Variation	T_c [°C]	C_s [kg/m ³]	k_h [m/d]	k_v [m/d]	λ_s [W/m °C]	c_{ps} [J/kg °C]	θ [dimensionless]
1	(Ref.)	80	35	15	1.5	3	800	0.35
2.1	$T_c = 0.5T_c^{ref}$	<u>40</u>	35	15	1.5	3	800	0.35
2.2	$T_c = 0.67T_c^{ref}$	<u>60</u>	35	15	1.5	3	800	0.35
2.3	$C_s = 1.33C_s^{ref}$	<u>100</u>	35	15	1.5	3	800	0.35
3.1	$C_s = 1/35C_s^{ref}$	80	<u>1</u>	15	1.5	3	800	0.35
3.2	$C_s = 10/35C_s^{ref}$	80	<u>10</u>	15	1.5	3	800	0.35
3.3 ^a	$C_{tr} = 1/35C_s^{ref}$	80	<u>1</u>	15	1.5	3	800	0.35
4.1	$k_h = 0.33k_h^{ref}$	80	35	<u>5</u>	<u>0.5</u>	3	800	0.35
4.2	$k_h = 3.0k_h^{ref}$	80	35	<u>45</u>	<u>4.5</u>	3	800	0.35
4.3	$k_v = 5k_v^{ref}$	80	35	15	<u>7.5</u>	3	800	0.35
5.1	$\lambda_s = 0.67\lambda_s^{ref}$	80	35	15	1.5	<u>2</u>	800	0.35
5.2	$\lambda_s = 1.33\lambda_s^{ref}$	80	35	15	1.5	<u>4</u>	800	0.35
6.1	$c_{ps} = 0.9c_{ps}^{ref}$	80	35	15	1.5	3	<u>720</u>	0.35
6.2	$c_{ps} = 1.1c_{ps}^{ref}$	80	35	15	1.5	3	<u>880</u>	0.35
7.1	$\theta = 0.6\theta^{ref}$	80	35	15	1.5	3	800	<u>0.21</u>
7.2	$\theta = 1.2\theta^{ref}$	80	35	15	1.5	3	800	<u>0.42</u>

^a For Case 3.3, a non-linear density–temperature relation was used without taking in account the density effects of the tracer concentration (C_{tr}).

Table 3

Hydraulic and thermal aquifer properties used for all simulations.

Properties	Parameter value
Specific storage	$S_s = 1 \cdot 10^{-4} \text{ m}^{-1}$
Solid phase density	$\rho_s = 2650 \text{ kg/m}^3$
Heat capacity of the fluid	$c_{pf} = 4186 \text{ J/kg } ^\circ\text{C}$
Thermal conductivity of the fluid	$\lambda_f = 0.580 \text{ W/m } ^\circ\text{C}$
Molecular diffusion	$D_m = 8.64 \cdot 10^{-5} \text{ m}^2/\text{d}$
Longitudinal dispersivity	$\alpha_l = 0.5 \text{ m}$
Transversal dispersivity	$\alpha_T = 0.05 \text{ m}$

persivity value (α_l) of 0.5 m and a transverse dispersivity value (α_T) of 0.05 m were chosen, resulting in a grid Peclet number of 1 near the wellbore. SEAWAT uses a single set of dispersivity values which are applied to both heat and solute transport.

2.5. Metrics to quantify overall salinization and compare scenario results

The distribution of salt in the top of the aquifer (upper 25 m) was used to quantify the salinization and to facilitate comparison of the scenarios. Several metrics were defined for this purpose.

2.5.1. Cumulative salt mass and its associated center of mass

The transport of salt was quantified using the cumulative amount of salt mass in the upper 25 m of the aquifer and the associated center of mass. The cumulative salt mass is calculated using a summation over the salt mass in each grid cell in the model domain (725 columns, 100 layers):

$$M_T = \theta \sum_{j=0}^{725} \sum_{k=1}^{100} C(r, z) (r_{j+1}^2 \pi z_k - r_j^2 \pi z_k) \quad (9)$$

where M_T is the cumulative salt mass (kg), r_j is the radial distance at column j (m), and z_k is the depth at layer k (m). The following equations give the coordinates r_{cM} and z_{cM} (m) of the center of mass of the salt mass M_T from Eq. (9):

$$r_{cM} = \left(\theta \sum_{j=0}^{725} \sum_{k=1}^{100} C(r, z) (r_{j+1}^2 \pi z_k - r_j^2 \pi z_k) r_{j+1} \right) / M_T$$

$$z_{cM} = \left(\theta \sum_{j=0}^{725} \sum_{k=1}^{100} C(r, z) (r_{j+1}^2 \pi z_k - r_j^2 \pi z_k) z_k \right) / M_T \quad (10)$$

2.5.2. Maximum radius of salinization

We used the maximal radial extent of salt concentrations above 0.1 kg/m³ (100 ppm) close to the top of the aquifer (R_{max} at $z = 1 \text{ m}$) to quantify the maximum spreading of salt mass in the lateral direction.

2.5.3. Dimensionless analysis of thermo-haline convection

A dimensionless analysis is applied on the cases in the sensitivity analysis (Table 2) in order to characterize the buoyancy forces in our system. Both the temperature and the salt concentration affect the buoyancy term in the flow equation [4].

To determine the ratio between the buoyancy tendency due to the salt concentration contrast and the buoyancy tendency due to the temperature contrast, the Turner, or buoyancy, number is used [4]:

$$B = \frac{\Delta \rho_s}{\Delta \rho_T} \quad (11)$$

where $\Delta \rho_T$ is the maximum change in fluid density due to temperature (kg/m³) and $\Delta \rho_s$ is the maximum change in fluid density due to solute concentration (kg/m³). The dimensionless sensitivity analysis for all scenarios is listed in Table 4.

Table 4

The maximum change in fluid density due to temperature contrasts ($\Delta \rho_T$), the maximum change in fluid density due to salt concentration contrasts ($\Delta \rho_s$) and the associated buoyancy number for each scenario.

Case	Parameter	$\Delta \rho_T$ [kg/m ³]	$\Delta \rho_s$ [kg/m ³]	B [dimensionless]
1	Ref	27.13	27.15	1.00
2.1	$T_c = 40 \text{ } ^\circ\text{C}$	6.71	27.15	4.05
2.2	$T_c = 60 \text{ } ^\circ\text{C}$	15.67	27.15	1.73
2.3	$T_c = 100 \text{ } ^\circ\text{C}$	40.63	27.15	0.67
3.1	$C_s = 1 \text{ kg/m}^3$	27.13	7.76	0.29
3.2	$C_s = 10 \text{ kg/m}^3$	27.13	0.785	0.03
4.1	$k_h = 5 \text{ m/d}$	27.13	27.15	1.00
4.2	$k_h = 45 \text{ m/d}$	27.13	27.15	1.00
4.3	$k_v = 7.5 \text{ m/d}$	27.13	27.15	1.00
5.1	$\lambda_s = 2 \text{ W/m } ^\circ\text{C}$	27.13	27.15	1.00
5.2	$\lambda_s = 4 \text{ W/m } ^\circ\text{C}$	27.13	27.15	1.00
6.1	$c_{ps} = 720 \text{ J/kg } ^\circ\text{C}$	27.13	27.15	1.00
6.2	$c_{ps} = 880 \text{ J/kg } ^\circ\text{C}$	27.13	27.15	1.00
7.1	$\theta = 0.21$	27.13	27.15	1.00
7.2	$\theta = 0.42$	27.13	27.15	1.00

3. Results

First, the results for the reference scenario simulated with both the standard linear density equation of state and the newly implemented non-linear one are presented. Subsequently, the results of the sensitivity analysis (Table 2) are presented.

3.1. Reference scenario (Case 1)

In the reference scenario (Case 1), the effect of heat transfer from a hot well casing with a constant effective temperature of 80 °C for 40 years is simulated for a condition of fresh (0 kg/m³) groundwater overlying groundwater with a seawater salt concentration (35 kg/m³, Table 2).

3.1.1. Predicted salinization with linear and non-linear density equation of state

Case 1 is the simulation of the reference scenario with the non-linear density equation (Eq. (8)). The results show that density-driven upward groundwater flow along the wellbore induced by heat transfer from the well casing led to considerable salinization of the initially fresh upper part of the aquifer after 30 years (Fig. 5). Two distinct thermal convection cells developed: one in the dense, salt water at the bottom of the aquifer and another one in the fresh water. The radial extent of these convection cells increases over time due to the continuous heat transfer from the well casing. After hot saline groundwater reaches the top of the aquifer, it is transported laterally. It then gradually cools down and dilutes by mixing with the cooler, fresh, groundwater.

The total salt mass in the top 25 m appears to increase exponentially with time until it reaches a linear trend after 30 years, with a rate of ~4000 kg/year (Fig. 6A). The distance of the center of salt mass and the maximum lateral spreading of salinization (R_{max}) show a rapid initial increase after which the increase tapers down (Fig. 6B and C).

Modeling of the reference scenario (Case 1) was also done at different grid size ($dr = 0.33 \text{ m}$ by $dz = 0.33 \text{ m}$) for $[0.5 < r < 154]$ and $dr = 1 \text{ m}$ by $dz = 0.33 \text{ m}$ for $[154 < r < 500]$ to investigate the impact of grid resolution on the model results. The effects on the main metrics to quantify overall salinization (Section 2.5) are small, resulting in error percentages of total cumulative salt mass and associated center of mass in the range of 0.18–1.95% and 0.33–1.02% respectively. Therefore, no further grid refinement was done and the grid configuration described in Section 2.4 and was used for all simulations.

Case 1.1 is the reference scenario simulated with a linear density equation. A $\delta\rho/\delta C$ gradient of 0.73 was used for the linear salt

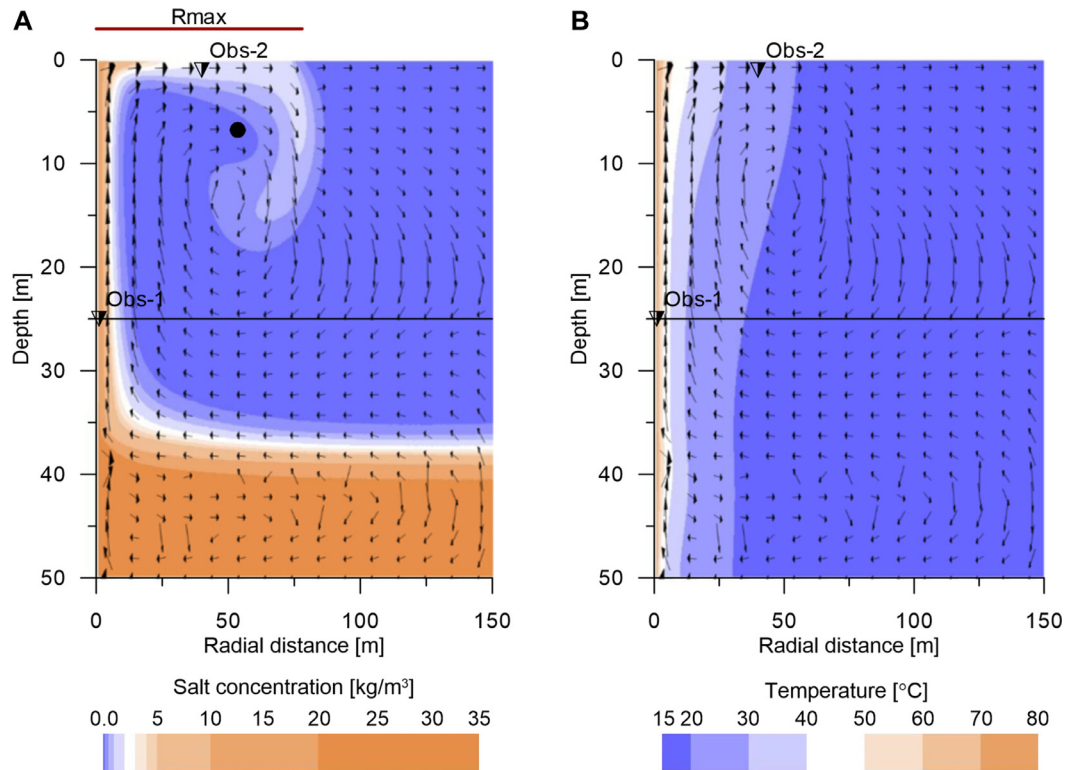


Fig. 5. (A) Salt concentrations [kg/m³] and (B) temperature [°C] at $t = 30$ years for the non-linear reference scenario (Case 1) with the Darcy velocity vectors. The dot shows the center of mass of cumulative stored salt in the model domain above the line $[0 < z < 25 \text{ m}]$ over time and the red line shows R_{max} . (For interpretation of the references to color in this figure legend, the reader is referred to the web version of this article.)

concentration–density relationship (Eq. (7)) and a $d\rho/dT$ gradient of -0.434 for the linear density–temperature relationship (line 1.1, Fig. 2). The results of this simulation reveal trends similar to those of the non-linear equation (Fig. 6). However, the linear density equation results in significant overestimation of the cumulative salt mass: 140,437 kg after 30 years instead of 70,867 kg (Fig. 6A). The relative error percentage for the cumulative salt mass increases from 81% after 5 years up to 103% after 40 years, respectively. Also the lateral spreading in the top of the aquifer is significantly overestimated while using the linear density equation. For instance, the r -coordinate of the center of mass and the maximum lateral spreading of salinization after 30 years is respectively 66.1 m and 103.5 m in the linear density case instead of 53.6 m and 78 m in the non-linear density case (Fig. 6B and C). The average relative error percentages for r -coordinate of the center of mass and R_{max} are respectively 24% and 32%.

The observed overestimation can be explained by the differences in the developed density gradients between the two cases. At the lower end of the groundwater temperature range, the density–temperature gradient for the non-linear density function is significantly lower than for the linear density approximation (line 1.1, Fig. 2). Consequently, the upward advective salt mass transport at low temperature ranges are significantly overestimated by the linear case (Case 1.1). Therefore, the associated mobilization of salt water occurs over a consistently larger radial distance from the wellbore. In addition to differences in upward advective salt mass transport, discrepancies in salt mass transport between the cases with linear and non-linear density equation of state are affected by differences in salt water mixing by dispersion at the fresh-salt water interface. Different lateral transport lengths and flow velocities along the fresh-salt water interface lead to variable extents of dispersive salt mixing.

It should be noted that convection is determined by the overall density distribution that is affected by both temperature and salt concentration contrasts. Thermal retardation plays an important role in

the difference between advective salt transport and heat transport during thermo-haline convection [30]. Salt mass is approximately transported at the pore velocity (q/θ), while heat is retarded due to thermal equilibration between the water and the solid grains (see Eq. (4)). Note that the salt water front at R_{max} has moved along both borehole length and the top of the aquifer, while the heat front has only moved along the top of the aquifer. Consequently, the thermal front moves much slower laterally away from the wellbore in the top of the aquifer than the salt front (as illustrated by Fig. 5). This means that at larger radial distance the vertical stabilizing temperature gradient on density decreases, and therefore the destabilizing gradient of salt concentration on density increases. If this destabilizing gradient of salt concentration is high enough and the horizontal flow velocity is low enough, downward transport of salt mass occurs at R_{max} (Fig. 5A). The lower density–temperature gradient in the temperature range of 15–20 °C for the non-linear density equation (Case 1) compared to the linear density approximation (Case 1.1) (line 1.1, Fig. 2), results in a faster destabilizing effect of the salt concentration gradient on water density at closer radial distances from the well for Case 1. Therefore, lateral transport of salt mass in the top of the aquifer (R_{max}) is overestimated for the linear density equation.

3.1.2. Reference scenario: breakthrough curves

Two observation points were added to the reference scenario to illustrate how the salinization and heating of the groundwater progress over time. Obs-1 is placed at a radial distance of 0.75 m from the wellbore, at a depth of 25 m and Obs-2 at a radial distance of 40 m from the wellbore in the upper 1 m of the aquifer (see Fig. 5). The upward transport of saline groundwater results in a progressively increasing but slightly fluctuating salt concentration in the vicinity of the wellbore (Fig. 7A). The salt concentration over time in Obs-1 increases from 4.7 kg/m³ (4700 ppm) after 1.5 years to 16.5 kg/m³ (16,500 ppm) after 40 years. The groundwater temperature in Obs-1

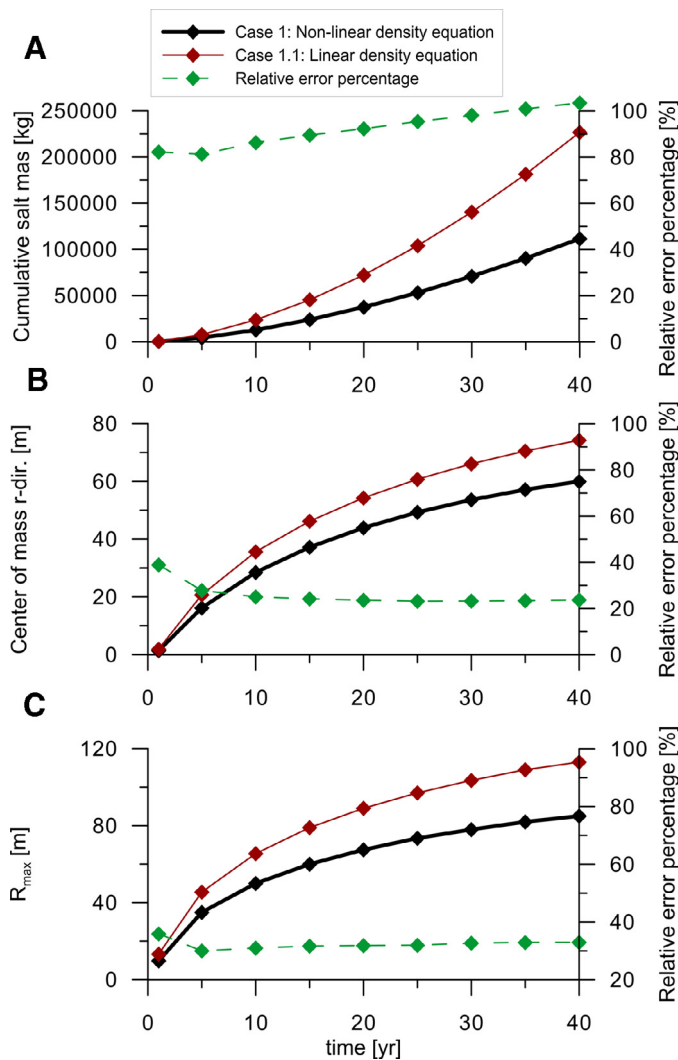


Fig. 6. (A) Cumulative salt mass, (B) associated center of mass and (C) the maximum spreading of salt mass in the lateral direction, R_{max} , in the upper half of the aquifer ($0 < r < 500$ m), ($0 < z < 25$ m) for the non-linear density scenario (Case 1) and the linear density scenario (Case 1.1). The relative error percentage between Case 1 and Case 1.1 is used to quantify the overestimation of these parameters while using the linear density equation.

reaches steady state in 1 year and remains constant at a temperature of 70.5 °C (Fig. 7A). Consequently, the upward Darcy velocity in Obs-1 after 1.5 years is 0.059 m/day and decreases slightly due to the increasing salt concentration and density of the groundwater (Fig. 8). At a radial distance of 4.75 m, no elevated salt concentrations breakthrough occurs and the upward Darcy velocity increases up to a value of 0.011 m/day after 10 years in the fresh water layer. The strength of the lower salt water thermal convection cell is significantly lower, resulting in upward Darcy velocities which are a factor 0.52 lower than observed in the fresh water layer at a radial distance of 4.75 m.

In the shallow observation point Obs-2 (Fig. 7B) elevated temperature breakthrough occurs after 3.7 years, while elevated salt concentrations (at 0.1 kg/m³) breakthrough occurs after 6.7 years. In the observation point Obs-2, the salt concentrations vary strongly over time between values of 2.00 (2000 ppm) and 2.45 kg/m³ (2450 ppm) after 30 years. Moreover, the variability in salt concentrations increases over time (Fig. 7B).

3.2. Parameter sensitivity analysis

Sensitivity analysis was conducted to test how the salinization is affected by various factors. A set of 6 parameters was varied with re-

spect to the reference scenario which is shown in Table 2. Three different temperatures at the well casing (Case 2) were simulated, as well as three different salt concentration contrasts with the overlying fresh water (Case 3), two hydraulic conductivities (Case 4), two thermal conductivities (Case 5), two solid phase heat capacities (Case 6), and two porosities (Case 7).

3.2.1. Effect of well casing temperature (Case 2)

The well temperature at shallow depth can vary over a wide range, depending on the technical application of the well as well as its production depth and insulation. In the simulations, the rate of salt mass transport and lateral spreading in the top of the aquifer were clearly affected by different effective well casing temperatures (Fig. 9). The highest casing temperatures resulted in the strongest increase in vertical transport and lateral spreading of salt mass in the upper part of the aquifer (Fig. 9). For a casing temperature of 100 °C (Case 2.3), the temperature is high enough to overcome the density difference between saline and fresh water ($B = 0.67$, Table 4). Consequently, advective transport of salt mass was observed along the whole well-bore length. This was not observed for Cases 1, 2.1 and 2.2, where the buoyancy number $B < 1$ (Table 4). The accumulation of transported salt mass into the top of the aquifer is disproportionately large with respect to the increases in effective temperature of the well casing. For example, the increase of temperature from 40 to 60 °C yields a 6.2–9 fold increase in total salt mass transport over the whole time range. In contrast, the lateral salt spreading increases progressively less at higher well casing temperatures. Low well casing temperatures ($T_c = 40$ °C) already result in distinct lateral spreading of salt mass in the top of the aquifer (Case 2.1) (Fig. 10).

3.2.2. Effect of salt concentration contrast (Case 3)

The reference scenario (Case 1) has fresh groundwater ($C_s = 0$ kg/m³) overlying water with a salt concentration of 35 kg/m³, which is representative of intruding seawater in coastal areas (e.g. [48]). However, smaller salt concentration contrasts may be present, e.g. due to long-term progressive salinization [33]. Cases 3.1 and 3.2 have salt concentration contrasts of 1 and 10 kg/m³, respectively. The rate of salt mass transport for Case 3.1 is only a factor 2.1 lower than for Case 1, while for Case 3.2 it is approximately a factor 1.2 higher (Fig. 11A). Although salt mass transport is highest for a salt concentration contrast of 10 kg/m³, the lateral spreading, as reflected by the radial center of mass and R_{max} , is slightly higher for the case with a lower (1 kg/m³) salt concentration contrast (Fig. 11B and C).

Two convection cells developed in the reference scenario (Case 1). In contrast, upward convective flow is not restricted at the fresh-salt interface for Cases 3.1 and 3.2. The buoyancy numbers B for both Cases 3.1 and 3.2 are lower than 1 (Table 4). Hence, the well casing temperature of 80 °C is sufficiently high to decrease the density of the water with a salt concentration of 1 or 10 kg/m³ below that of the initially fresh water density at 15 °C in the vicinity of the well-bore. Therefore, the saline groundwater moves upward over the entire thickness of the aquifer (Fig. 12A).

The stabilizing effect of salt concentration on the density contrasts is not taken into account for Case 3.3. The effect on the cumulative salt mass transport is the same as for Case 3.1 (Fig. 11A). However, lateral spreading of salt mass in the top of the aquifer was a factor 1.1 higher for Case 3.3 than for Case 3.1 (Figs. 11C and 12). Hence, the destabilizing effect of the salt concentration on density contrasts during lateral transport of salt mass in Case 3.1 results in a smaller radial extent of the convection cell over time compared to Case 3.3.

3.2.3. Effect of hydraulic conductivity (Case 4)

The hydraulic conductivity of the aquifer influences groundwater flow velocities. Decreasing k_h and k_v values by a factor of 3 (Case 4.1), the cumulative salt mass transported into the top of aquifer decreases

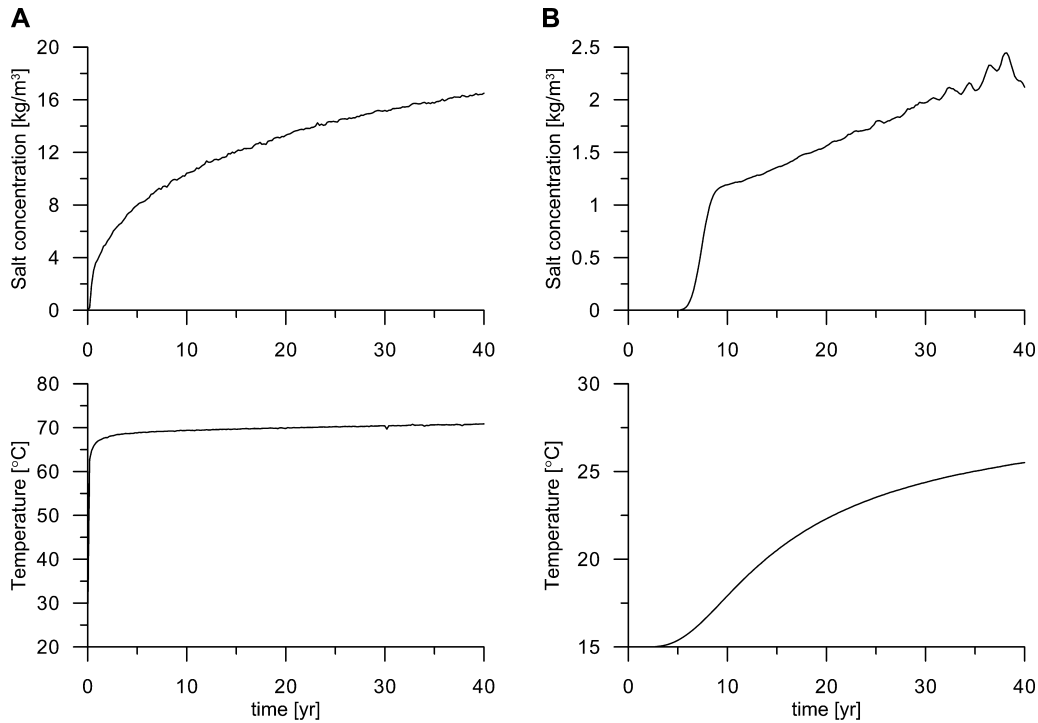


Fig. 7. Breakthrough curves at observation points (A) Obs-1 and (B) Obs-2 for respectively salt concentration and temperature for the reference scenario (Case 1).

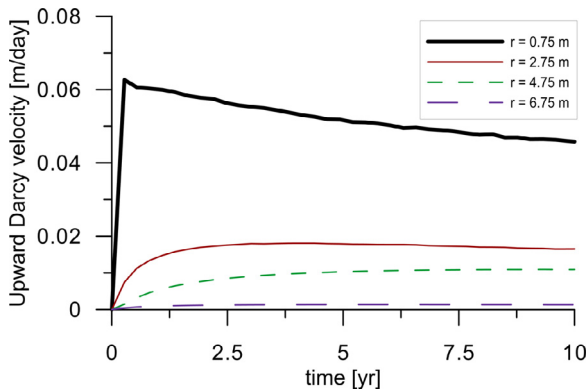


Fig. 8. Upward Darcy velocity over time at different radial distances in the vicinity of the wellbore 25 m depth.

by a factor of 3.0 compared to the reference case (Fig. 13). The contrary is observed for Case 4.2, where k_h and k_v are increased by a factor of 3. This results in increased cumulative salt mass in the top of aquifer by a factor of 2.5. Case 4.3 has a higher anisotropy ratio, where k_v is raised to 7.5 m/day. This results in the largest salt mass transported into the top of the aquifer after 15 years of all considered scenarios. The downward transport of salt mass at the outer boundary of the convection cell is also increased for both Cases 4.2 and 4.3 and salt water is already transported to a depth below 25 m after 24 and 17 years, respectively. Consequently, continuous salt mass loss out of the upper aquifer domain [$0 < z < 25$ m] results in a slower increase of cumulative salt mass for these cases (Fig. 13A and B).

3.2.4. Different thermal properties of the aquifer (Cases 5 and 6)

The thermal conductivity and heat capacity of the solid phase influence heat transport via the bulk thermal diffusivity term (Eq. (3)) and the thermal retardation factor (Eq. (5)), respectively. A higher thermal conductivity of the solid phase increases the heat conduction from the well casing to the aquifer and the density-driven groundwater flow. Varying the thermal conductivity for the solid phase within

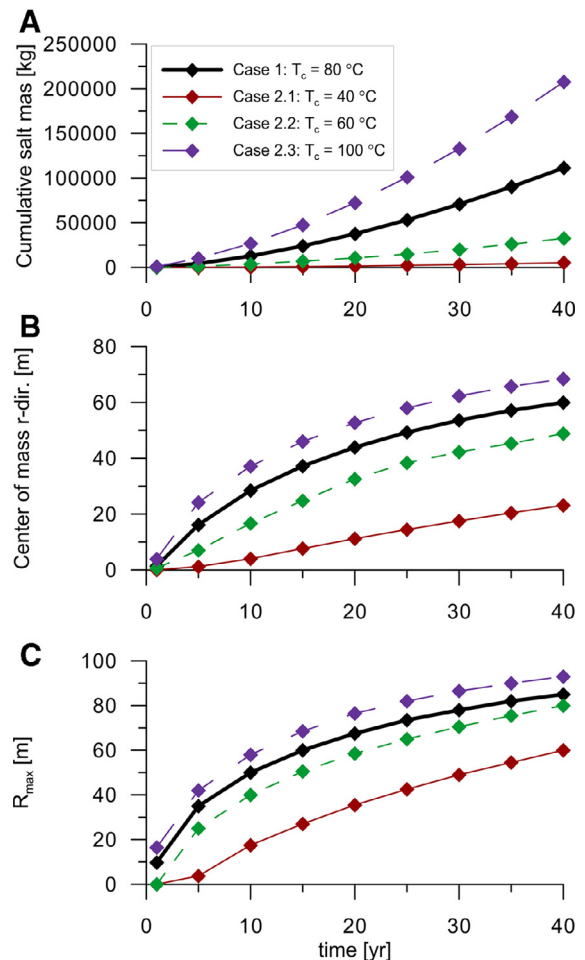


Fig. 9. (A) Cumulative salt mass, (B) associated center of mass and (C) R_{max} in the upper half of the aquifer [$0 < r < 500$ m], [$0 < z < 25$ m] for Case 2.

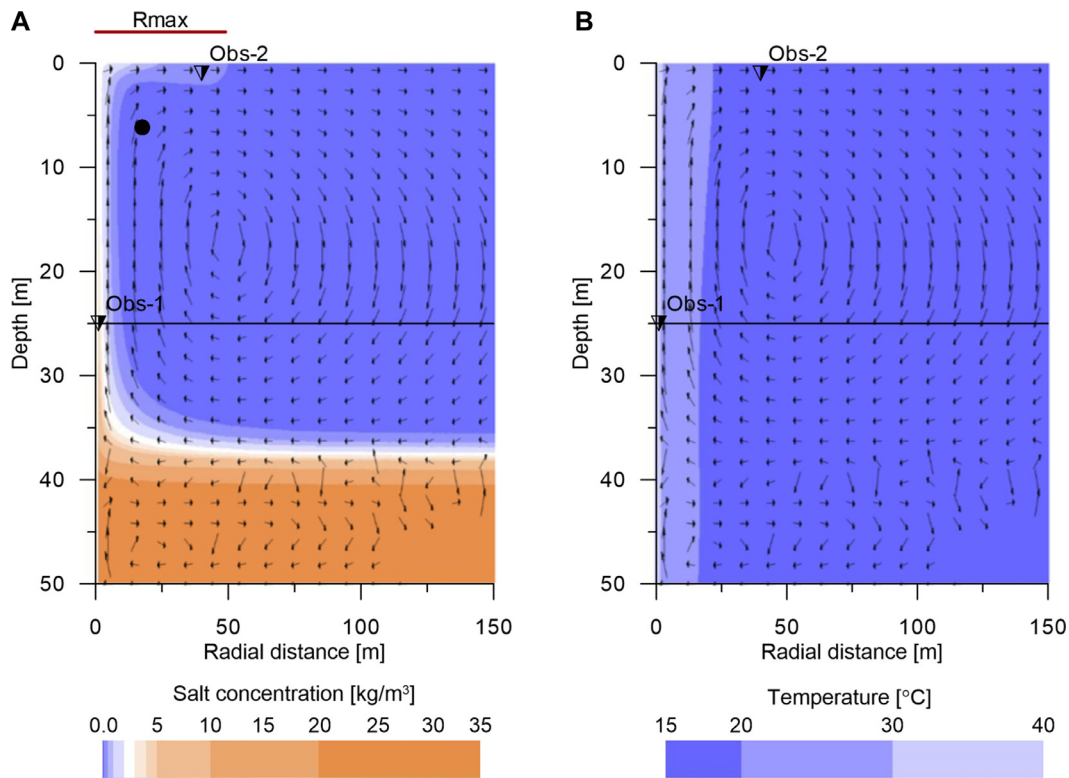


Fig. 10. (A) Salt concentrations [kg/m³] and (B) temperature [°C] at $t = 30$ years for the scenario with a well casing temperature of 40 °C (Case 2.1) with the Darcy velocity vectors. The dot shows the center of mass of cumulative stored salt in the model domain above the line $[0 < z < 25 \text{ m}]$ over time and the red line shows R_{max} . (For interpretation of the references to color in this figure legend, the reader is referred to the web version of this article.)

a realistic range showed a moderate impact on the convection. The salt mass transported into the top of the aquifer increased by a factor of 1.2 for the upper bound (Case 5.2) and decreased by a factor of 1.2 for the lower bound (Case 5.1) after 30 years (Fig. 13).

Besides thermal conduction, heat transport is determined by thermal retardation which is described as a function of the heat capacity of the solid (Eq. (5)). The effect of thermal retardation is small (Case 6). A higher heat capacity of the solid (Case 6.2) resulted in more absorption of heat into the solid matrix during heat transport and thereby a higher thermal retardation factor. Consequently, the salt front moves faster laterally away from the well than the thermal front and cooling of the salt front occurs at closer radial distances from the well. This results in a faster destabilizing effect of the salt concentration gradient on water density during lateral salt transport and hence a reduced maximal lateral spreading (R_{max}). The reverse is observed for Case 6.1, since the adsorption of heat into the solid matrix is lower than the reference scenario.

3.2.5. Effect of aquifer porosity (Case 7)

Porosity affects heat transport by bulk thermal diffusivity (Eq. (3)) and thermal retardation (Eq. (5)). SEAWATv4 allows only modeling with effective porosity, while heat conduction is determined by the overall, bulk porosity. Hence, thermal conduction in the aquifer will be slightly overestimated when considering effective porosity instead of bulk porosity, since the bulk thermal diffusivity term (D_T) will be lower in the simulations. The total cumulative salt mass in the top of the aquifer for Case 7 indicates that the parameter sensitivity for varying porosity is high (Fig. 13). The lowering of the porosity by a factor of 0.6 (Case 7.1) increased the salt mass transport by a factor of 1.14. An increased porosity by a factor 1.2 results in decreased salt mass transport by a factor of 1.04. The decrease and increase in salt mass transport are mainly due to the difference in advective salt mass transport. For Case 7.1, the pore velocity (q/θ) at a given Darcy velocity

is increased by a factor 1.7, while for Case 7.2 the pore velocity is decreased by a factor 1.2. In reality such porosity changes would likely be accompanied by permeability changes that mitigate the impact of porosity.

4. Discussion

Simulations show that the heat loss from well casings can induce upward convection of salty groundwater, leading to salinization of overlying fresh groundwater. To the best of our knowledge, this is the first study that considers the impact of hot well casings on groundwater flow and salt concentration gradients in aquifers. Here, the practical implications, such as monitoring requirements and the implications of modeling density-driven flow under the conditions presented in this study will be discussed.

4.1. Implementation of non-linear density equation of state

We have simulated density-driven flow over large temperature and salt concentration ranges induced by the heat transfer from a hot well casing. The resulting salt and heat transport in the aquifer was shown to occur over relatively short distances ($< 100 \text{ m}$). The implementation of a non-linear density equation of state [38] in SEAWAT was required for accurate results, as the linear approximation causes relative errors up to 103% for the cumulative salt mass transport. Other numerical simulations of convection induced by temperature gradients use a non-linear relation between density and temperature only (e.g. [15,42]). This study uses a non-linear density dependence on both salt concentration and temperature.

Generally, heat transport mechanisms are classified as natural (free) convection if flow is solely induced by fluid density differences and forced convection if flow is forced by external sources, like a hydraulic gradient. Previous studies have shown that heat transport

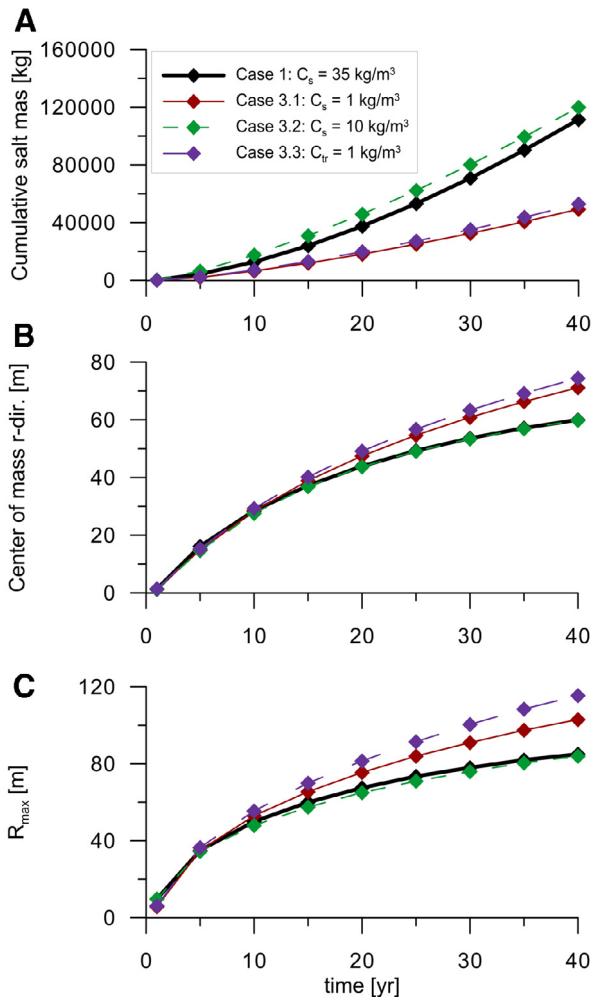


Fig. 11. (A) Cumulative salt mass, (B) associated center of mass and (C) R_{\max} in the upper half of the aquifer [$0 < r < 500 \text{ m}$], [$0 < z < 25 \text{ m}$] for Case 3.

by forced convection over relative small time ranges can be simulated with linear density approximations in the SEAWAT code (e.g. [25,44]). However, in the present study, heat transport is solely due to free convection under the influence of continuous heat conduction from the well casing over a large time range (up to 40 years). The radial temperature distribution in the model domain varies spatially and temporally. No sharp temperature front between the hot water mass and colder ambient groundwater is observed (shown in Fig. 5B). Both temperature and salt concentration distributions determine the extent of the convection cells and the associated convective transport over time. This is reflected in the difference between the simulations with linear and non-linear density relations (Fig. 6).

A non-linear density relation in SEAWAT enables numerical simulations of problems where thermally induced free convection in aquifers occurs over large temperature and time ranges. A disadvantage would be the increased run times associated with the use of a non-linear density relation. The higher accuracy of the implemented non-linear density equation comes at the price of a larger computational runtime: 50 h compared to 20 for Case 1.1 with a Core i7-4770@3.40 GHz processor.

4.2. Well casing temperatures of exploration wells

The range of well casing temperatures used in this study is representative for temperatures encountered for conventional oil and gas wells, geothermal energy production, as well as hot water or steam

injection [6,11,13,35,50]. However, little information is available on the actual temperature at the outside of the well casing. The actual temperature is an important parameter changing for different practical applications. This means that for a specific production or injection operation detailed information about the wellhead temperature over depth, the thermal resistance of the well system and the actual temperature gradient over time in the well system is required to simulate heat transfer into the aquifer as accurately as possible.

Decline in production rates results in decreasing well casing temperatures. Therefore, the effects of thermally induced density-driven groundwater flow on upward salt transport are expected to be lower when the duration of heat transfer through the wellbore decreases to a few years. For example, typical initial shale gas production rates of major U.S. shale gas fields are around 30 million m^3 per year, while production rates drops to values around 4 million m^3 per year after 5 years of operation [43]. The analytical function by Ramey [35] predicts that such low production rates will result in small temperature differences ($< 5^\circ\text{C}$) between the wellbore fluid and the shallow aquifer.

4.3. Fresh-salt interfaces and salt concentration contrasts

Fresh-salt interfaces are common in coastal areas (e.g. [48]). In general, these interfaces have relative small dispersed transition zones between fresh and saline waters compared to other stratified fresh-salt aquifer systems. Usually, coastal regions are densely populated and fresh water reserves are scarce. Salinization poses problems for drinking water, agriculture, and ecological habitats [34,48]. This study can be used to provide insight into possible thermal impacts on groundwater flow and salinization risks near deep wells penetrating fresh water lenses.

Fresh-salt groundwater stratification also occurs in regions with brackish paleo-groundwater, or halite-rich formations [5,33]. For these scenarios, the lower salt concentration contrasts of 1 and 10 kg/m^3 (Cases 3.1 and 3.2) are realistic. However, a less sharp dispersed fresh-salt transition should be considered under these conditions [33]. Salt mass transport from the upper part of the diffusive transition zone could then occur at lower temperature contrasts. For example, for Case 3.2, the salt concentrations in the upper part of a diffusive transition interface will be lower compared to a case with a sharp salt concentration contrast of 10 kg/m^3 . Consequently, the required temperature rise to overcome the buoyancy difference with cold fresh groundwater will be lower. Therefore, it is likely that salt transport occurs over a larger radial distance along the wellbore if a wide diffusive fresh-salt transition zone is considered.

Moreover, direct upward salt transport over the entire aquifer thickness occurs for the lower salt concentration contrasts (1 and 10 kg/m^3) of Cases 3.1 and 3.2 (Section 3.2.2). The density difference for the reference scenario is too large to allow direct groundwater flow along whole borehole length at the simulated effective well casing temperatures (Cases 1 and 2.1–2.3). Consequently, the effect of salt mixing by dispersion between the salt and fresh water layer along the fresh-salt interface becomes more important for this case with two separate convection cells.

4.4. Uncertainties in the simulation results

Dispersion along the fresh-salt interface controls the salt transport to the top of the aquifer for large salt concentration contrasts when two convection cells develop (e.g. Case 1). Such enhanced salt water mixing along a fresh-salt water interface due to the formation of thermal convection cells was observed in the lab experiment of Henry and Hilleke [14] and numerical simulations of this experiment [25]. In this experiment, warm fresh water was injected in a large sand-filled tank and flowed on top of water with a salt concentration of 35 kg/m^3 . Heat pads were located at the lower and right part of the

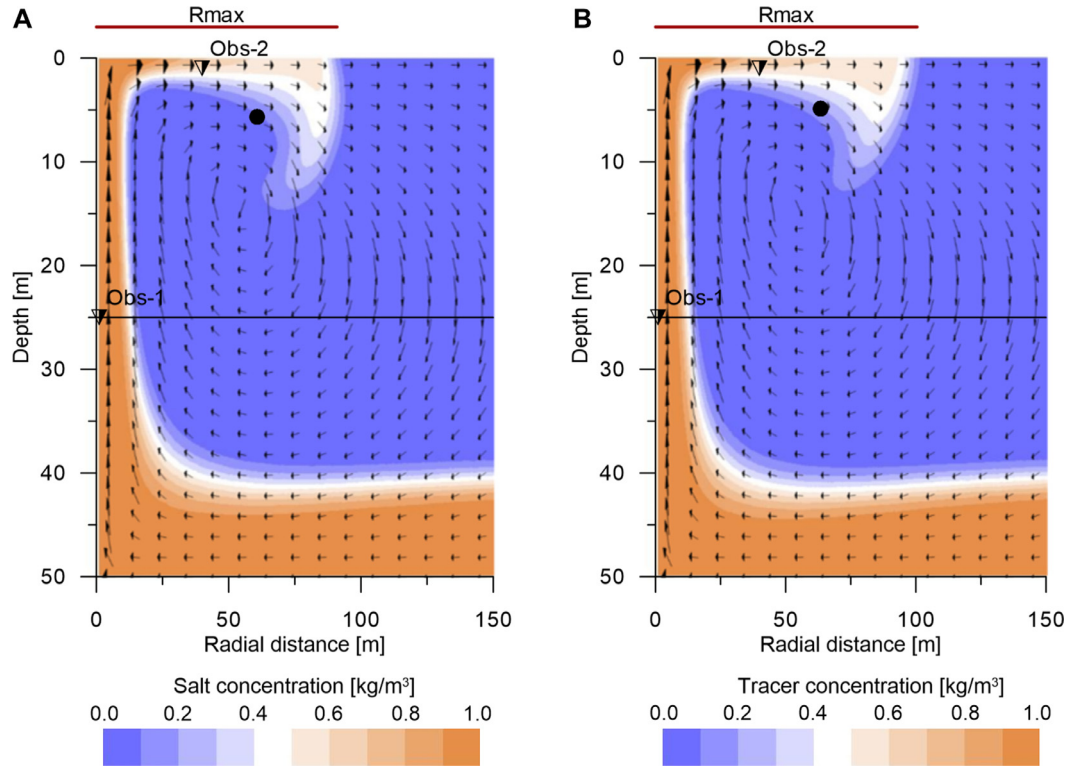


Fig. 12. (A) Salt concentrations [kg/m³] for Case 3.1 and (B) salt concentrations [kg/m³] for Case 3.3 at $t = 30$ years with the Darcy velocity vectors. The dots show the center of mass of cumulative stored salt in the model domain above the line $[0 < z < 25 \text{ m}]$ over time and the red line shows R_{\max} . (For interpretation of the references to color in this figure legend, the reader is referred to the web version of this article.)

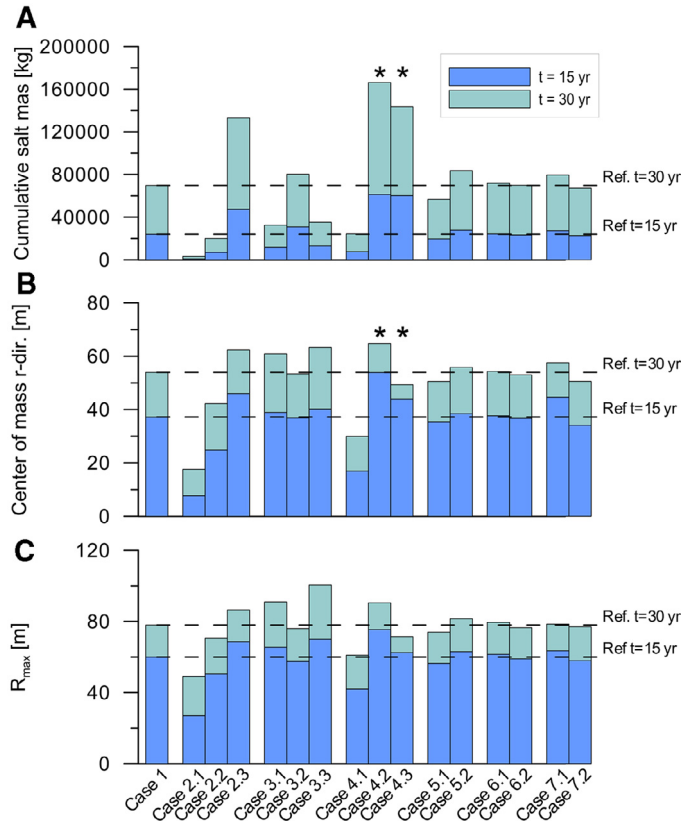


Fig. 13. Sensitivity of the (A) cumulative salt mass, (B) associated center of mass, and (C) R_{\max} in the upper half of the aquifer $[0 < r < 500 \text{ m}]$, $[0 < z < 25 \text{ m}]$ after 15 and 30 years. *Note that for Cases 4.2 and 4.3 salt has been transported downward, below the 25 m reference line at the outside of the convection cell.

sand-filled tank, resulting in thermal convection cells in the lower left part of the tank in both the fresh and the salt water layer. The mixing by these convection cells widened the fresh-salt interface. For a simulation scenario without taking into account the temperature dependency of the density, less salt mass transport was observed due to the absence of thermal convection cells.

This illustrates that the mixing along a fresh-salt interface is largely controlled by advection and transverse dispersion [4,31]. The presented simulations used dispersivity values of $\alpha_l = 0.5 \text{ m}$ and $\alpha_T = 0.05 \text{ m}$. Enhanced solute mixing by dispersion will result in increased salt mass transport to the top of the aquifer. For example, a scenario with dispersivity values of $\alpha_l = 1.0 \text{ m}$ and $\alpha_T = 0.1 \text{ m}$ resulted in an increase in salt mass transport by a factor of 1.14. Therefore, the dispersivity value should be carefully considered for simulations of specific field cases with fresh-salt interfaces (e.g. [9]).

Small fluctuations of salt concentrations with time are observed in the vicinity of the wellbore, when the salt concentration contrast of the interface is large (such as in Case 1, Fig. 7A). This can be explained by the difference in diffusivity between heat and salt. The initial situation is stable due to the salt concentration gradient. The heat transfer from the wellbore causes destabilization of the system. This is called the diffusive regime of Double Diffusive Convection and instabilities can arise during this phenomenon [4]. At the top, hot salt water moves laterally over colder fresh water. This is called the fingering regime of Double Diffusive Convection [4,17,39]. If the destabilizing salt concentration gradient in the top of the aquifer is large (e.g. Case 1 and Case 3.2), it results in instabilities and fluctuating salt concentrations over time (Fig. 7B). The salt concentration fluctuations due to Double Diffusive Convection decreases with enhanced salt mixing by dispersion.

Grid resolution, dispersivity values, and the use of a 2D axisymmetric domain could have an effect on the simulation of unstable upward fluid flow along the wellbore and local salt concentration fluctuations (e.g. [4,19]). Therefore, the salt concentrations should be

measured frequently in the field (e.g. using automatic electrical conductivity (EC) data loggers) to obtain insight in the mixing and the average salt concentrations at the top of the aquifer.

This study did not consider heat loss from the aquifer into the confining layers. Horizontal heat transport from hot well casings to surrounding aquitards will be conduction dominated, while heat transport in the aquifer occurs by both conduction and convection. As illustrated in Fig. 5B, the upward convective heat transport results in heat accumulation and hence a larger radius of elevated aquifer temperature at the top of the aquifer. The radius of elevated aquifer temperature at the bottom of the aquifer is reduced by the convective inflow of cooler native groundwater. Heat conduction into and from the aquifer can be expected for the underlying and overlying aquitards, respectively. However, the thermal conductivity is generally high for clay layers compared to the thermal conductivity of sandy aquifers [1,7]. Hence, heat transfer from the well casing into the aquitard by thermal conduction is expected to be higher than for the aquifer. Therefore, heat conduction into the aquitard is expected to have a limited impact on the lateral transport of salt in the top of the aquifer.

4.5. Practical considerations

The present study shows the possibility of significant upward transport of salt around hot well casings. Field evidence of this phenomenon does not exist to the best of our knowledge. This would require spatially detailed and frequent long-term monitoring to obtain quantitative insight on such thermo-haline convection in the vicinity of hot wells. The simulations of the present study were carried out for an axi-symmetric homogeneous sandy confined aquifer domain. This section addresses the implications of different field conditions.

Axi-symmetric flow condition strongly reduces simulation running times, but does not allow simulation of regional groundwater flow. However, regional flow will increase the net heat transfer from the hot well casing to ambient groundwater and cause a different temperature distribution around the well. This will change the thermal convection cells in both salt and fresh water layer.

The aquifer was assumed to be homogeneous. However, variations in hydraulic and thermal properties of the aquifer near the wellbore would impact the density-driven groundwater flow and salt mass transport. Aquifer heterogeneity could have a large impact on convective flow patterns in thermo-haline systems [28]. For example, horizontal clay lenses restrict density-driven flow and may lead to separate convection cells above and below a clay lens. Consequently, salinization of the upper part of the aquifer might be limited or even prevented.

Unconfined aquifers were not tested in this study. For an unconfined aquifer, the temperature at the water table is controlled by the atmospheric temperature. Continuous heat loss at the top results in less intensive convection. Consequently, salt mass transport and lateral spreading of salt in the top of the phreatic zone are expected to be lower as for confined aquifers. In addition, unconfined aquifers are recharged with fresh water by precipitation which will dilute transported salt water in the top of the phreatic zone.

5. Conclusions

To the best of our knowledge, this is the first study that shows that heat loss from well casings may cause mixing due to density-driven flow and mobilize fresh-salt water interfaces, resulting in salinization of shallow fresh groundwater. A non-linear density relationship as a function of both salt concentration and temperature had to be implemented in the SEAWATv4 code to simulate this phenomenon accurately. The total transported salt mass to the top of the aquifer ranged between values of 3150 and 166,000 kg after 30 years for the simulated scenarios. Lateral spreading of salt mass in the top of the aquifer

occurred over radial distances up to 91 m. During lateral transport of salt water along the top of the aquifer, fluctuating salt concentration breakthrough over time occurs due to destabilizing salt concentration gradients.

For large salt concentration contrasts, such as a fresh-salt (seawater) interface, groundwater heating results in the formation of separate convection cells in the fresh water layer and the salt water layer. At smaller salt concentration contrasts, the heated salt water layer becomes less dense than the cooler native groundwater. Hence, upward advective transport of salt along the wellbore occurs over the entire thickness of the aquifer.

The convection and salt transport is stronger for scenarios with increased temperatures of the well casing, increased horizontal and vertical hydraulic conductivities, decreased porosity and increased thermal conductivity of the aquifer. Therefore, these aspects should be considered when assessing the potential impact of hot well casings for site-specific conditions. The results of this study indicate heat loss from hot well casings can induce density-driven groundwater flow and salinization of shallow fresh groundwater. This process should therefore be considered when monitoring for long-term groundwater quality changes near wells through which hot fluids or gases are transported.

Acknowledgments

The authors thank four anonymous reviewers for their constructive feedback, which allowed us to improve the manuscript significantly.

Appendix A. Modified density equation in SEAWAT

The calculation steps for the density calculation (Fig. 4) are outlined in this appendix. The non-linear density equation (Eq. (8)) has been implemented in the VDF package of SEAWAT. The code for the function CALCDENS in the VFD1.f file has been adapted. This function calculates fluid density for each grid cell from the concentrations of each MT3DMS species, which is in our model salt concentration (C_s) and temperature (T).

First the salt concentration (in kg/m³) and temperature (in °C) are read. Subsequently, the iterative algorithm is performed by solving Eqs. (A.1)–(A.3):

$$S = C_s / \rho_{n-1} \quad (\text{A.1})$$

$$\begin{aligned} \rho_n = & (999.9 + 2.034 \cdot 10^{-2} T - 6.162 \cdot 10^{-3} T^2 \\ & + 2.261 \cdot 10^{-5} T^3 - 4.657 \cdot 10^{-8} T^4) \\ & + \left(802.0 \frac{S}{1000} - 2.001 \frac{S}{1000} T + 1.677 \cdot 10^{-2} \frac{S}{1000} T^2 \right. \\ & \left. - 3.060 \cdot 10^{-5} \frac{S}{1000} T^3 - 1.613 \cdot 10^{-5} \frac{S}{1000}^2 T^2 \right) \quad (\text{A.2}) \end{aligned}$$

$$r_\rho = |\rho_n - \rho_{n-1}| \quad (\text{A.3})$$

Closure of the iterative scheme is set to residual $r_\rho < 1 \cdot 10^{-3}$.

References

- [1] Bear J. *Dynamics of fluids in porous media*. New York: Dover Publications; 1972.
- [2] Buscheck TA, Doughty C, Tsang CF. Prediction and analysis of a field experiment on a multilayered aquifer thermal energy storage system with strong buoyancy flow. *Water Resour Res* 1983;19(5):1307–15 <http://dx.doi.org/10.1029/WR019i005p01307>.
- [3] Cheng P, Minkowycz WJ. Free convection about a vertical flat plate embedded in a porous medium with application to heat transfer from a dike. *J Geophys Res* 1977;82(14):2040–4 <http://dx.doi.org/10.1029/JB082i014p02040>.
- [4] Diersch HJG, Kolditz O. Variable-density flow and transport in porous media: approaches and challenges. *Adv Water Resour* 2002;25(8–12):899–944 [http://dx.doi.org/10.1016/S0309-1708\(02\)00063-5](http://dx.doi.org/10.1016/S0309-1708(02)00063-5).

- [5] Edmunds WM, Hinsby K, Marlin C, Condeso de Melo MT, Manzano M, Vaikmae R, Travi Y. Evolution of groundwater systems at the European coastline. *Geol Soc Spec Publ* 2001;189:289–311 <http://dx.doi.org/10.1144/GSL.SP.2001.189.01.17>.
- [6] Eickmeier JR, Ersoy D, Ramey Jr HJ. Wellbore temperatures and heat losses during production or injection operations. *J Can Pet Tech* 1970;9(2):115–21 <http://dx.doi.org/10.2118/70-02-08>.
- [7] Engineering T. 2007, The engineering toolbox: tools and basic information for design, engineering and construction of technical applications. <http://www.engineeringtoolbox.com/>, last accessed 27-9-2014.
- [8] Fitts CR. *Groundwater science*. San Diego: Academic Press; 2002.
- [9] Gelhar LW, Welty C, Rehfeldt KR. A critical review of data on field scale dispersion in aquifers. *Water Resour Res* 1992;28(7):1955–74 <http://dx.doi.org/10.1029/92WR00607>.
- [10] Guo W, Langevin CD. User's guide to SEAWAT: a computer program for simulation of three-dimensional variable-density ground-water flow. *Techniques of water-resources investigations 6-A-7*. US Geological Survey; 2002.
- [11] Hagoot J. Prediction of wellbore temperatures in gas production wells. *J Pet Sci Eng* 2005;49(1–2):22–36 <http://dx.doi.org/10.1016/j.petrol.2005.07.003>.
- [12] Harbaugh AW, Banta ER, Hill MC, McDonald MG. MODFLOW-2000, the US Geological Survey modular ground-water models. User guide to modularization concepts and the ground-water flow process. Open-file report 00-92. US Geological Survey; 2000.
- [13] Hassan AR, Kabir CS. Modeling two phase fluid and heat flows in geothermal wells. *J Pet Sci Eng* 2010;71(1–2):77–86 <http://dx.doi.org/10.1016/j.petrol.2010.01.008>.
- [14] Henry H.R., Hilleke J.B. Exploration of multiphase fluid flow in a saline aquifer system affected by geothermal heating. University of Alabama Bureau of Engineering Research Contract No. 14-08-0001-12681. U.S. Geological Survey; 1972 (submitted for publication).
- [15] Holzbecher E. Numerical studies on thermal convection in cold groundwater. *Int J Heat Mass Transf* 1997;40(3):605–12 [http://dx.doi.org/10.1016/0017-9310\(96\)00133-0](http://dx.doi.org/10.1016/0017-9310(96)00133-0).
- [16] Hughes JD, Langevin CD, Brakefield-Goswami L. Effect of hypersaline cooling canals on aquifer salinization. *Hydrogeol J* 2010;18(1):25–38 <http://dx.doi.org/10.1007/s10040-009-0502-7>.
- [17] Imhoff PT, Green T. Experimental investigation of double-diffusive ground-water fingers. *J Fluid Mech* 1988;188:363–82 <http://dx.doi.org/10.1017/S002211208800076X>.
- [18] Isdale JD, Morris R. Physical properties of sea water solutions: density. *Desalination* 1972;10(4):329–39 [http://dx.doi.org/10.1016/S0011-9164\(00\)80003-X](http://dx.doi.org/10.1016/S0011-9164(00)80003-X).
- [19] Jamshidzadeh Z, Tsai FTC, Mirbagheri SA, Ghasemzadeh H. Fluid dispersion effects on density-driven thermohaline flow and transport in porous media. *Adv Water Resour* 2013;61:12–28 <http://dx.doi.org/10.1016/j.advwatres.2013.08.006>.
- [20] Kipp K.L., HST3D: A computer code for simulation of heat and solute transport in three-dimensional ground-water flow systems. *Water resources investigations report 86-4095*. U.S. Geological Survey; 1987.
- [21] Kolditz O, Ratke R, Diersch HJG, Zielke W. Coupled groundwater flow and transport: 1. Verification of variable density flow and transport models. *Adv Water Resour* 1998;21(1):27–46 [http://dx.doi.org/10.1016/S0309-1708\(96\)00034-6](http://dx.doi.org/10.1016/S0309-1708(96)00034-6).
- [22] Kutasov AM. Dimensionless temperature, cumulative heat flow and heat flow rate for a well with a constant bore-face temperature. *Geothermics* 1987;16(5–6):467–72 [http://doi:10.1016/0375-6505\(87\)90032-0](http://doi:10.1016/0375-6505(87)90032-0).
- [23] Langevin CD. Modeling axisymmetric flow and transport. *Ground Water* 2008;46(4):579–90 <http://dx.doi.org/10.1111/j.1745-6584.2008.00445.x>.
- [24] Langevin C.D., Thorne D.T., Jr., Dausman A.M., Sukop M.C., Guo W. SEAWAT Version 4: a computer program for simulation of multi-species solute and heat transport. In: *Techniques and Methods 6-A22*. U.S. Geological Survey; 2008.
- [25] Langevin CD, Dausman AM, Sukop MC. Solute and heat transport model of the Henry and Hilleke laboratory experiment. *Ground Water* 2010;48(5):757–70 <http://dx.doi.org/10.1111/j.1745-6584.2009.00596.x>.
- [26] Millero FJ, Poisson A. International one-atmosphere equation of state of seawater. *Deep-Sea Res* 1981;28A(6):625–9 [http://dx.doi.org/10.1016/0198-0149\(81\)90122-9](http://dx.doi.org/10.1016/0198-0149(81)90122-9).
- [27] Molz F.J., Melville J.G., Parr A.D., King D.A., Hopf M.T. Aquifer thermal energy storage: a well doublet experiment at increased temperatures. *Water Resour Res* 1983;19(1):149–60. <http://dx.doi.org/10.1029/WR019i001p0149>.
- [28] Musuuza J.L., Radu FA, Attinger S. Predicting predominant thermal convection in thermohaline flows in saturated porous media. *Adv Water Resour* 2012;49:23–36 <http://dx.doi.org/10.1016/j.advwatres.2012.07.020>.
- [29] Nield DA. Onset of thermohaline convection in a porous medium. *Water Resour Res* 1968;4(3):553–60 <http://dx.doi.org/10.1029/WR004i003p00553>.
- [30] Oldenburg CM, Preuss K. Plume separation by transient thermohaline convection in porous media. *Geophys Res Letters* 1999;26(19):2997–3000 <http://dx.doi.org/10.1029/1999GL002360>.
- [31] Oswald SE, Kinzelbach W. Three-dimensional physical benchmark experiments to test variable-density flow models. *J Hydrol* 2004;290(1–2):22–42 <http://dx.doi.org/10.1016/j.jhydrol.2003.11.037>.
- [32] Pop I, Sunanda JK, Cheng P, Minkowycz WJ. Conjugate free convection from long vertical plate fins embedded in a porous medium at high Rayleigh numbers. *Int J Heat Mass Transf* 1985;28(9):1629–36 [http://dx.doi.org/10.1016/0017-9310\(85\)90137-1](http://dx.doi.org/10.1016/0017-9310(85)90137-1).
- [33] Post VEA. Groundwater salinization processes in the coastal area of the Netherlands due to transgressions during the Holocene [Ph.D. thesis]. Earth and Life Science Department, Free University of Amsterdam: The Netherlands; 2004.
- [34] Post VEA, Abaraca E. Preface: saltwater and freshwater interactions in coastal aquifers. *Hydrogeol J* 2010;18(1):1–4 <http://dx.doi.org/10.1007/s10040-009-0561-9>.
- [35] Ramey Jr HJ. Wellbore heat transmission. *J Pet Tech* 1962;14(4):427–35 <http://dx.doi.org/10.2118/96-PA>.
- [36] Rubin H, Roth C. On the growth of instabilities in groundwater due to temperature and salinity gradients. *Adv Water Resour* 1979;2:69–76 [http://dx.doi.org/10.1016/0309-1708\(79\)90013-7](http://dx.doi.org/10.1016/0309-1708(79)90013-7).
- [37] Safarov J, Millero F, Feistel R, Heintz A, Hassel E. Thermodynamic properties of standard seawater extensions to high temperatures and pressures. *Ocean Sci* 2009;5:235–46.
- [38] Sharqawy MH, Lienhard VJH, Zubair SM. Thermophysical properties of seawater: a review of existing correlations and data. *Desalin Water Treat* 2010;16(1–3):354–80 <http://dx.doi.org/10.5004/dwt.2010.1079>.
- [39] Taunton JW, Lightfoot EN, Green T. Thermohaline instability and salt fingers in a porous medium. *Phys Fluids* 1972;15(5):748–53 <http://dx.doi.org/10.1063/1.1693979>.
- [40] Thorne D, Langevin CD, Sukop MC. Addition of simultaneous heat and solute transport and variable fluid viscosity to SEAWAT. *Comput Geosci* 2006;32(10):1758–68 <http://dx.doi.org/10.1016/j.cageo.2006.04.005>.
- [41] Tilton LW, Taylor JK. Accurate representation of the refractivity and density of distilled water as a function of temperature. *J Res Nat Bur Stand* 1937;18:205–14.
- [42] Tsang CF, Buscheck T, Doughty C. Aquifer thermal energy storage: a numerical simulation of Auburn University field experiments. *Water Resour Res* 1981;17(3):647–58 <http://dx.doi.org/10.1029/WR017i003p00647>.
- [43] Energy Information Administration U.S. Annual energy outlook 2012 with projections to 2035. DOE/EIA-0383(2012). Washington, DC: U.S. Energy Information Administration; 2012. <http://www.eia.gov/forecasts/aeo/pdf/0383%282012%29.pdf> [accessed 25.06.14].
- [44] Vandenbohede A, Hermans T, Nguyen F, Lebbe L. Shallow heat injection and storage experiment: heat transport simulation and sensitivity analysis. *J Hydrol* 2011;409(1–2):262–72 <http://dx.doi.org/10.1016/j.jhydrol.2011.08.024>.
- [45] Vandenbohede A, Louwyck A, Vlamynck N. SEAWAT-based simulation of axisymmetric heat transport. *Ground Water* 2013;52(6):908–15 <http://dx.doi.org/10.1111/gwat.12137>.
- [46] Voss CI. A finite-element simulation model for saturated-unsaturated, fluid-density-dependent ground-water flow with energy transport or chemically-reactive single-species solute transport. *Water resources investigations report 84-4369*. U.S. Geological Survey; 1984.
- [47] Wallis L, Prommer H, Post V., Vandenbohede A., Simmons C.T. Simulating MODFLOW-based reactive transport under radially symmetric flow conditions. *Ground Water* 2013;51(3):398–413. <http://dx.doi.org/10.1111/j.1745-6584.2012.00978.x>.
- [48] Werner AD, Bakker M, Post VAE, Vandenbohede A, Lu C, Ataie-Ashtiani B, Simmons CT, Barry DA. Seawater intrusion processes, investigation and management: Recent advances and future challenges. *Adv Water Resour* 2013;51:3–26 <http://dx.doi.org/10.1016/j.advwatres.2012.03.004>.
- [49] Wooding RA. Steady state free thermal convection of liquid in a saturated permeable medium. *J Fluid Mech* 1957;2(3):273–85 <http://dx.doi.org/10.1017/S0022112057000129>.
- [50] Wu YS, Pruess K. An analytical solution for wellbore heat transmission in layered formations. *SPE Reserv Eng* 1990;5(4):531–8 <http://dx.doi.org/10.2118/17497-PA>.
- [51] Zheng C., Wang P.P. MT3DMS: A modular three-dimensional multispecies transport model for simulation of advection, dispersion and chemical reactions of contaminant in ground-water systems; documentation and user's guide. Contract report SERDP-99-1. U.S. Army Corps of Engineer Research and Development Center; 1999.